IOP PUBLISHING PHYSICS IN MEDICINE AND BIOLOGY

Phys. Med. Biol. **54** (2009) 4225–4241 doi:10.1088/0031-9155/54/13/017

Thermal interaction of short-pulsed laser focused beams with skin tissues

Jian Jiao and Zhixiong Guo[1]

Department of Mechanical and Aerospace Engineering, Rutgers, The State University of New Jersey, Piscataway, NJ 08854, USA

E-mail: guo@jove.rutgers.edu

Received 22 February 2009, in final form 25 May 2009
Published 17 June 2009
Online at stacks.iop.org/PMB/54/4225

Abstract

Time-dependent thermal interaction is developed in a skin tissue cylinder subjected to the irradiation of a train of short laser pulses. The skin embedded with a small tumor is stratified as three layers: epidermis, dermis and subcutaneous fat with different optical, thermal and physiological properties. The laser beam is focused to the tumor site by an objective lens for thermal therapy. The ultrafast radiation heat transfer of the focused beam is simulated by the transient discrete ordinates method. The transient Pennes bio-heat equation is solved numerically by the finite volume method with alternating direction implicit scheme. Emphasis is placed on the characterization of the focused beam propagation and absorption and the temperature rise in the focal spot. The effects of the focal spot size and location, the laser power, and the bio-heat equation are investigated. Comparisons with collimated irradiation are conducted. The focused beam can penetrate a greater depth and produce higher temperature rise at the target area, and thus reduce the possibility of thermal damage to the surrounding healthy tissue. It is ideal for killing cancerous cells and small tumors.

(Some figures in this article are in colour only in the electronic version)

1. Introduction

Basal cell carcinoma (BCC) is the most common skin cancer in humans. It develops from basal cells, which are in the deepest layer of the epidermis (Gilchrest *et al* 1999). Each year in the United States, about 900 000 people are diagnosed with basal cell carcinoma (550 000 male, 350 000 female). The estimated lifetime risk of basal cell carcinoma in the white population is 33–39% for men and 23–28% for women.

[1] Author to whom any correspondence should be addressed.

It has been well established that organic tissue responds strongly to temperature rise. The thermal impact on tissue changes drastically when temperature exceeds 43 °C; the rate of 'cell kill' doubles for every 1 °C increase beyond 43 °C and decreases by a factor of 4–6 for every 1 °C drops below 43 °C (Jeong *et al* 2003). It has also been noticed that tumor cells are more sensitive to temperature increase than normal tissues (Anghileri and Robert 1986). Moreover, Robinson *et al* (1998) found that a temperature evaluation to at least 56 °C for 1 s or more was sufficient to bring about cancer cell denaturation and death.

Lasers have been widely considered in clinical therapies (Anderson and Parrish 1983, Amin *et al* 1993, Manns *et al* 1999) and applications (Yamada 1995, Niemz 2002), including laser-induced hyperthermia, laser-induced interstitial thermotherapy, interstitial laser photocoagulation therapy, laser microsurgery, as well as optical imaging (Hebden *et al* 1997, Yamada 2000, Gao *et al* 2004, Guo *et al* 2006). The objective of hyperthermia in cancer treatment is to raise the temperature in cancerous tissue above a therapeutic value while maintaining the surrounding healthy tissue at sub-lethal temperature values in cases where surgical intervention is dangerous. In order to more effectively destroy/detect cancerous tissues, contrast agents such as absorbing and/or fluorescing dyes can be administrated for enhancement of light absorption (Ntziachristos *et al* 2000, Quan and Guo 2004).

Ultrafast lasers output ultra-short pulses with pulse width in the range from picoseconds down to femtoseconds. Due to the extremely short pulse duration, which is much shorter than the thermal relaxation time of many materials, beam interaction with a material occurs before heat diffusion in the material ever takes place, leading to increased local temperature in a very short time period and minimization of the heat-affecting zone. This will lessen thermal damage to the surroundings, a concern that should always be born in mind in laser applications. With the use of an ultrafast laser, significant improvement in the damage localization over continuous wave and general pulsed lasers has been attained (Zysset *et al* 1989).

Two characteristics in ultrafast radiation heat transfer (Kim and Guo 2004) are worth mentioning. One is that the transient effect is significant when the pulse duration is not substantially longer than the characteristic time of radiation propagation in the medium. For applications in tissues where the typical characteristic thickness is in the order of millimeters to centimeters, the corresponding characteristic time (length over the speed of light) is in the range 0.01–1 ns. Hence, the propagation of an ultra-short pulse with the speed of light must be incorporated into the equation of radiative transfer (Guo and Kumar 2002). Another characteristic is that the emission from the medium is generally negligible as compared with the high laser intensity. Thus, the medium is cold in the modeling of radiative heat transfer. Many methods were considered for modeling photon transport and migration in turbid media (Yamada 1995, Sassaroli *et al* 1999, Binzoni *et al* 2006). Mitra and Kumar (1999) compared several one-dimensional methods for simple plane wall problems. To accurately capture the propagation of a short pulse in multi-dimensional geometries, the authors' group has developed the transient Monte Carlo method (Guo *et al* 2000), the radiation element method (Guo and Kumar 2001a) and the transient discrete ordinates method (Guo and Kumar 2001b). Comparison with experiments has also been carried out (Guo and Kumar 2002, Wan *et al* 2004).

Accurate prediction of temperature distributions and heat transfer rates in tissues (Pfefer *et al* 2000, Zhu *et al* 2002, Kim and Guo 2007) is also paramount for clinical laser therapies and applications. The Pennes model that describes heat transfer in perfused tissues is a well-known bio-heat equation. It assumes that the thermal contribution of blood be modeled as if it entered an imaginary pool at equilibrium with the surrounding tissue. A recent review (Arkin *et al* 1994) compared several bio-heat models and concluded that the Pennes model is still the

most practical for fast prediction of transient temperature profiles such as those expected in certain hyperthermia conditions.

To maximize treatment efficacy and avoid undesirable reactions in normal tissues, thermal therapies ideally deliver heat to the target while spare the surrounding healthy tissue. As a non-invasive means to deliver energy to a location inside the body, the technique of converging beam can eliminate the perforation of skin. Moreover, due to concentrating the energy at the focal spot, a converging beam can penetrate a greater depth in the tissue without significant attenuation. A focused beam with a spot size comparable to cells is ideal for precisely killing cancerous cells without damaging surrounding healthy cells. This makes it very useful in the treatment of small tumors at the very early stage or as a supplemental method for killing precisely any leftover cancerous cells that may exist after surgical procedures. The temperature at the focal zone is higher than that of the surroundings, and it is then considered as the desired temperature for treatment or therapy. Therefore, accurate prediction of the focal zone temperature is critical. A literature survey reveals that complete thermal modeling of a focused beam in tissues has been rarely conducted.

In this work, a combined model of ultrafast radiative heat transfer and Pennes bio-heat transfer is developed to simulate the heat transfer processes in a model skin tissue subjected to the irradiation of a train of short pulses. The skin tissue is stratified as three layers with different properties. An inhomogeneity simulating a small skin tumor is embedded in the dermis layer beneath the skin surface. To effectively heat up the cancerous cells, a collimated laser beam is converged into the tumor site by a single objective lens. The laser beam is axisymmetric and has temporal and spatial Gaussian distributions. A technique for treating realistic beam convergence is introduced. Comparisons between the converging beam and collimated irradiation are conducted. The influences of the focal spot size, the laser power and the bio-heat equation are also scrutinized.

2. Mathematical formulation

2.1. Governing equations

A laser beam is focused at the small tumor in the skin tissue as shown in figure 1. The intensity I_l of the diffused radiation in a discrete ordinate $\overrightarrow{s_l}$ is described by the time-dependent equation of radiative transfer in cylindrical coordinates (Kim and Guo 2004):

$$\frac{1}{c}\frac{\partial I_l}{\partial t}+\frac{\mu_l}{r}\frac{\partial}{\partial r}(rI_l)-\frac{1}{r}\frac{\partial}{\partial \phi}(\eta_l I_l)+\xi_l\frac{\partial I_l}{\partial z}+\sigma_e I_l=\sigma_e S_l, \quad l=1,2,\ldots,M, \tag{1}$$

where μ_l, η_l, ξ_l are the three directional cosines, σ_e is the extinction coefficient, which is the summation of the absorption coefficient σ_a and scattering coefficient σ_s, c is the speed of light in the tissue, S_l is the radiative source term, which is

$$S_l=(1-\omega)I_b+\frac{\omega}{4\pi}\sum_{j=1}^{M}w_j\Phi_{jl}I_l+S_i^l, \tag{2}$$

in which I_b is the black body emitting intensity of the tissue, $\omega=\sigma_s/(\sigma_s+\sigma_a)$ is the scattering albedo, w_j is the appropriate angular weight in the discrete direction $\vec{s}_j$, Φ_{jl} represents the scattering phase function $\Phi(\vec{s}_j\rightarrow\vec{s}_l)$, and S_i^l is the source contribution of the laser irradiation and can be expressed as

$$S_i^l=\frac{1}{4\pi}I_i\Phi(\vec{s}_i\rightarrow\vec{s}_l), \tag{3}$$

where the unit vector $\overrightarrow{s_i}$ represents the laser incident direction. Light scattering in tissues is generally anisotropic (Binzoni *et al* 2006). However, it is reasonable to scaling down to

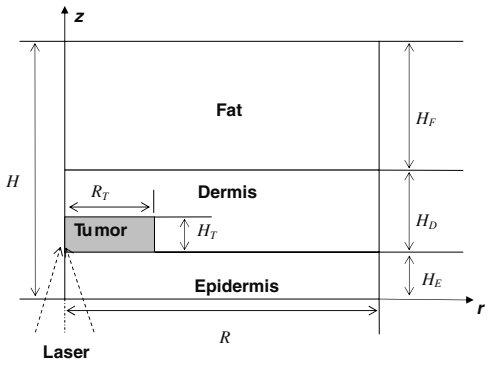

Figure 1. The skin geometry and the coordinates.

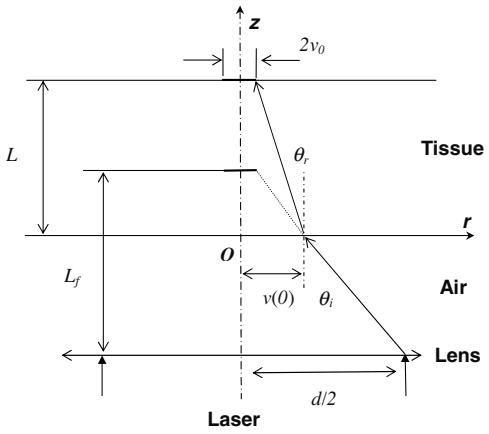

Figure 2. The laser beam convergence.

isotropic scattering (Guo and Kumar 2000). When the reduced scattering coefficient is used, the scattering phase function is unity. In the region where no laser irradiation is passing through, $I_i = S_i = 0$.

The intensity of a laser beam having a Gaussian profile both temporally and spatially can be expressed as

$$I_i(r, z, t) = (1 - R_0)I_0(z)\exp\{-4\ln 2 \times [(t - z/c)/t_p - 1.5]^2\} \times \exp[-2r^2/v(z)^2]\exp(-\sigma_e z), \quad (4)$$

where I_0 is the amplitude of the beam radiation strength, v is the beam radius ($1/e^2$), R_0 is the reflectance on the tissue–air interface, and t_p is the pulse width at half maximum. The total time duration of a whole pulse is set as 3 t_p in this study so that the peak of the pulse arrives at time 1.5 t_p. The impinging area of the beam considered is $r \leqslant v(z)$.

Because of the mismatch of refractive indices of the air and tissue, the incident laser beam is refracted at the tissue–air interface and will not converged to the focus of the lens in free space but rather to a deeper distance in the tissue as shown in figure 2. For a Gaussian beam, the radius of a diffraction-limit focal spot can be calculated as

$$v_0 = 1.22(\lambda L_f/d), \quad (5)$$

where λ is the laser wavelength, L_f is the focal length of the converging lens in free space, and d is the diameter of the collimated beam before the lens. The focal spot size is little affected by the refractive index of the medium to be focused to. For a focusing depth L in the medium, the radius of the impinging area on the medium surface is then obtained as

$$v(0) = L \cdot \tan\theta_r + v_0, \tag{6}$$

in which the refractive angle is obtainable by Snell's law:

$$\theta_r = \sin^{-1}\left(\frac{\sin\theta_i}{n}\right), \tag{7}$$

where n is the refractive index of the tissue and it is assumed to be 1.40. The incident angle of the focusing beam is

$$\theta_i = \tan^{-1}\left(\frac{d/2 - v_0}{L_f}\right). \tag{8}$$

Inside the tissue, the propagating beam radius varies with z:

$$v(z) = \frac{v(0) - v_0}{L}|z - L| + v_0. \tag{9}$$

The amplitude of the beam radiation strength is correlated with the laser beam power P at the tissue surface as

$$P = 0.46\pi v(z)^2 I_0(z) f t_p, \tag{10}$$

where f is the pulse repetition rate.

Once the intensity field is obtained, the incident radiation and the divergence of radiative heat flux can be calculated as

$$G = \sum_{l=1}^{n} w_l I_l + I_c, \tag{11}$$

$$\nabla \cdot q_{\text{rad}} = \sigma_a(4\pi I_b - G), \tag{12}$$

where I_c is normally incident laser intensity.

Because the pulse duration considered is much shorter than the thermal relaxation time of tissue, heat diffusion during the pulse irradiation period is negligible. Hence, the temperature rise in the tissue is due to the irradiation of an ultra-short pulse is described as

$$\rho C_P \frac{\partial T(r, z, t)}{\partial t} = -\nabla \cdot q_{\text{rad}}(r, z, t). \tag{13}$$

Between two successive pulses, heat diffusion is incorporated and Penne's equation (Arkin *et al* 1994) is used for modeling the bio-heat transfer in the skin tissue:

$$\rho C_p \frac{\partial T(r, z, t)}{\partial t} = k\nabla^2 T + (\rho C)_b \omega_b (T_a - T) + q_m, \tag{14}$$

where ρ, C_p, k,T denote the density, specific heat, thermal conductivity and temperature of tissue, respectively; C_b is the specific heat of blood, ω_b is the blood perfusion rate, q_m is the metabolic heat generation rate, and T_a is the supplying arterial blood temperature.

2.2. Boundary conditions

For the radiative heat transfer modeling, three types of radiation boundary conditions are considered for the present problem. At the laser incident surface ($z = 0$) Fresnel reflection must be considered because of the mismatch of the refractive indices between the tissue and air. For internal radiation at the tissue–air interface, a critical angle is given by Snell's law:

$$\theta_{\mathrm{cr}} = \sin^{-1}(1/n). \tag{15}$$

Total reflection occurs when the angle of incidence $\theta_i > \theta_{\mathrm{cr}}$. Otherwise, the reflection at the interface is purely specular and the reflectance is calculated by Fresnel's equation:

$$R_s = \frac{1}{2}\left[\frac{\tan^2(\theta_i - \theta_r)}{\tan^2(\theta_i + \theta_r)} + \frac{\sin^2(\theta_i - \theta_r)}{\sin^2(\theta_i + \theta_r)}\right]. \tag{16}$$

All other surfaces are tissue–tissue interface. Since biological tissues are highly scattering, photons reaching the boundary of a tissue must have been undergone multiple scattering events and the possibilities of photons passing through the boundary or reflecting back are almost equal for a turbid medium. Thus, we specify a diffuse reflectance $R_d = 0.5$ on such surfaces. The reflecting boundary condition at the wall is given by

$$I_w = R_s I_w^{-1} + \frac{R_d}{\pi}\left[I_{cw} + \sum_{\vec{s_l}\cdot\vec{n}<0} w_l I_{w,l} |\vec{s_l} \cdot \vec{n}|\right]. \tag{17}$$

The centerline of the tissue cylinder ($r = 0$) is specified as an axisymmetric boundary.

For the bio-heat transfer modeling, except for the laser incident surface which is exposed to the ambient air at room temperature $T_{\mathrm{am}} = 25\ ^\circ\mathrm{C}$ with the heat transfer coefficient $h = 15\ \mathrm{W}$ ($\mathrm{m}^{-2}\ \mathrm{K}^{-1}$), all other surfaces of the tissue cylinder are surrounded by other tissue remained at 37 °C. Again the centerline of the tissue cylinder is treated as the axisymmetric boundary. The initial and boundary conditions for the bio-heat transfer model are summarized below:

$$T = 37\,^\circ\mathrm{C}, \qquad \text{when } t = 0, \tag{18}$$

$$T = 37\,^\circ\mathrm{C}, \qquad \text{at } r = R \text{ or } z = H, \tag{19}$$

$$\frac{\partial T}{\partial r} = 0, \qquad \text{at } r = 0, \tag{20}$$

$$-k\frac{\partial T}{\partial z} = h(T_{\mathrm{am}} - T), \qquad \text{at } z = 0. \tag{21}$$

2.3. Properties of the model skin tissue and the laser parameters

In this model, human skin ($H = 10$ mm, $R = 10$ mm) is organized in distinct layers, which are epidermis ($H_E = 1$ mm), dermis ($H_D = 2$ mm) and subcutaneous fat ($H_F = 7$ mm), respectively. A small skin tumor ($H_T = 1$, $R_T = 1$ mm), either infiltrative basal cell carcinomas (IBCC) or nodular basal cell carcinomas (NBCC), is suited in the dermis layer. The IBCC-type tumor has a higher absorption coefficient than that of the NBCC-type tumor. Their thermal and physiological properties are assumed to be the same. The optical (at wavelengths 1200 nm and 1064 nm, respectively), thermal and physiological properties of the considered tissues are listed in tables 1–3, respectively.

Unless specified otherwise, the laser and lens parameters used in this work are as follows. The focal length of the converging lens is 10 mm in free space. The collimated laser beam diameter is 6 mm. The laser wavelength is centered at 1200 nm. At this wavelength light

Table 1. Optical parameters for different tissue layers at wavelengths 1200 nm and 1064 nm, respectively (Salomatina *et al* 2006).

Tissue type	Epidermis	Dermis	Fat	IBCC	NBCC
λ (nm)			1200/1064		
σ_s (mm^{-1})	2.6/3.0	1.7/1.83	1.5/1.69	1.05/1.22	1.0/1.11
σ_a (mm^{-1})	0.06/0.02	0.12/0.05	0.18/0.07	0.15/0.10	0.02/NA

Table 2. Thermal parameters for different tissue layers (Cohen 1977).

Tissue type	Epidermis	Dermis	Fat	Tumor
ρC_p (J mm^{-3} K^{-1})	4.2×10^{-3}	4.2×10^{-3}	4.2×10^{-3}	4.2×10^{-3}
k (W m^{-1} K^{-1})	0.21	0.30	0.21	0.59

Table 3. Physiological parameters for different skin tissue layers (Emery and Sekins 1982).

Tissue type	Epidermis	Dermis	Fat	Tumor
Perfusion ratio (ml ml^{-1} s^{-1})	0	1.63×10^{-3}	1.0×10^{-3}	5.0×10^{-3}
Metabolic heat generation (W kg^{-1})	1.0	1.0	0.32	0.67

absorption of the epidermis is low (Salomatina *et al* 2006) and the incident light may penetrate to the cancerous region. The focal spot has a beam diameter of approximately 5 μm. The average laser power is 0.065 W. The pulse width and repetition rate are 10 ps and 1 MHz, respectively. With these parametric values, the peak pulse power density at the focal spot 1–2 mm beneath the skin surface after attenuation is two to three orders of magnitude lower than the ablation threshold ($>10^{11}$ W cm^{-2}) in tissues (Niemz 2002). Thus, laser-induced ablation mechanism does not apply and the current thermal analysis fits in.

2.4. Numerical schemes

The transient discrete ordinates method (TDOM) with S_{10} scheme was employed for the solution of the present ultrafast radiative heat transfer problem. For detailed information on the numerical scheme and accuracy, please refer to the author Guo's previous publications (Guo and Kumar 2002, Kim and Guo 2004). As noted by Chai *et al* (1993) a ray effect exists because of limited number of discrete ordinates. In the literature, S_4 (24 discrete ordinates) and S_8 (80 discrete ordinates) schemes were commonly adopted. The strong directionality in focusing beam requires for high-order quadratures such as S_{10} (120 discrete ordinates). With S_{10}, the ray effect could be lessened (Guo and Kumar 2001b). The transient conductive heat transfer equations are solved numerically by using the alternating direction implicit (ADI) scheme (Anderson *et al* 1984) which is well known in computational physics, and thus, the details are not repeated here.

For both the radiation and conduction simulations, the same grid system is adopted to avoid interpolation. To improve the numerical calculation efficiency and to capture the rapid change in the focus, a non-uniform grid system is employed, with a refined grid in the focus region. For a typical skin tissue cylinder with $R = 10$ mm and $H = 10$ mm, the adopted staggered grid is 80×80 in the present calculations. The time step is 0.2 ps for the radiation calculation and 0.25 μs for the bio-heat conduction, respectively. Several sets of different

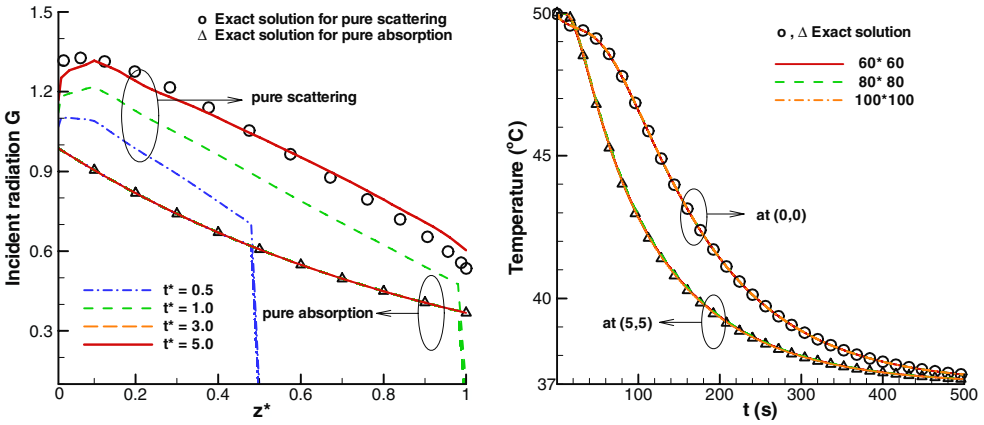

(a) **Validation of the radiation model.** (b) **Validation of the conduction model.**

Figure 3. Comparison between the exact solutions and the numerical predictions. (a) Validation of the radiation model. (b) Validation of the conduction model.

grid sizes and time steps were considered, and they could all give satisfactory and convergent results.

Since the optical and thermal properties of the tissue are assumed to be constant because the temperature is not dramatically changed during irradiation, the transient radiation heat transfer does not vary between pulses and it is only required to calculate the response of one pulse. The temperature rise obtained for this initial pulse can be applied to any subsequent pulse as a simple addition to the temperature field for the treatment of a pulse train. The bio-heat transfer process is simulated in the whole period of the pulse train until the cut-off of irradiation. For radiation transfer modeling, the computational time is about 30 min for one pulse irradiation using a DELL PC (Optiplex 755: 2.40 GHz CPU and 3.25 GB RAM).

3. Results and discussion

To validate the computational models, comparisons with exact solutions in simple situations are conducted. Wu and Wu (1997) considered a cylinder of unity optical length and unity aspect ratio. The medium in the cylinder was assumed to be gray and homogeneous, and the boundaries were assumed to be non-reflecting. A uniform collimated radiation with unity intensity was incident on the top of the cylinder. Two dimensionless variables were defined as $z^* = \sigma_e z$ and $t^* = ct/L$. The incident radiation profiles along the optical axis ($r = 0$) for both the pure absorption and purely scattering cases are shown in figure 3(a). For the pure scattering case, it is seen that the temporal profile of the incident radiation gradually reaches to the steady-state exact solution (Wu and Wu 1997) as time proceeds to $t^* = 5$ that is much longer than the pulse duration. For the pure absorption case, the present transient solution at $t^* = 5$ matches perfectly with the steady-state exact solution obtained by using the Beer–Lambert law.

The ADI method for heat conduction modeling is validated in a tissue cylinder that is assumed to have a uniform initial temperature 50 °C. In figure 3(b), the numerically predicted temperatures at the origin (0,0) and in a position (5 mm, 5 mm) are compared with the exact solutions that the authors obtained by using the method of separation of variables. It is seen

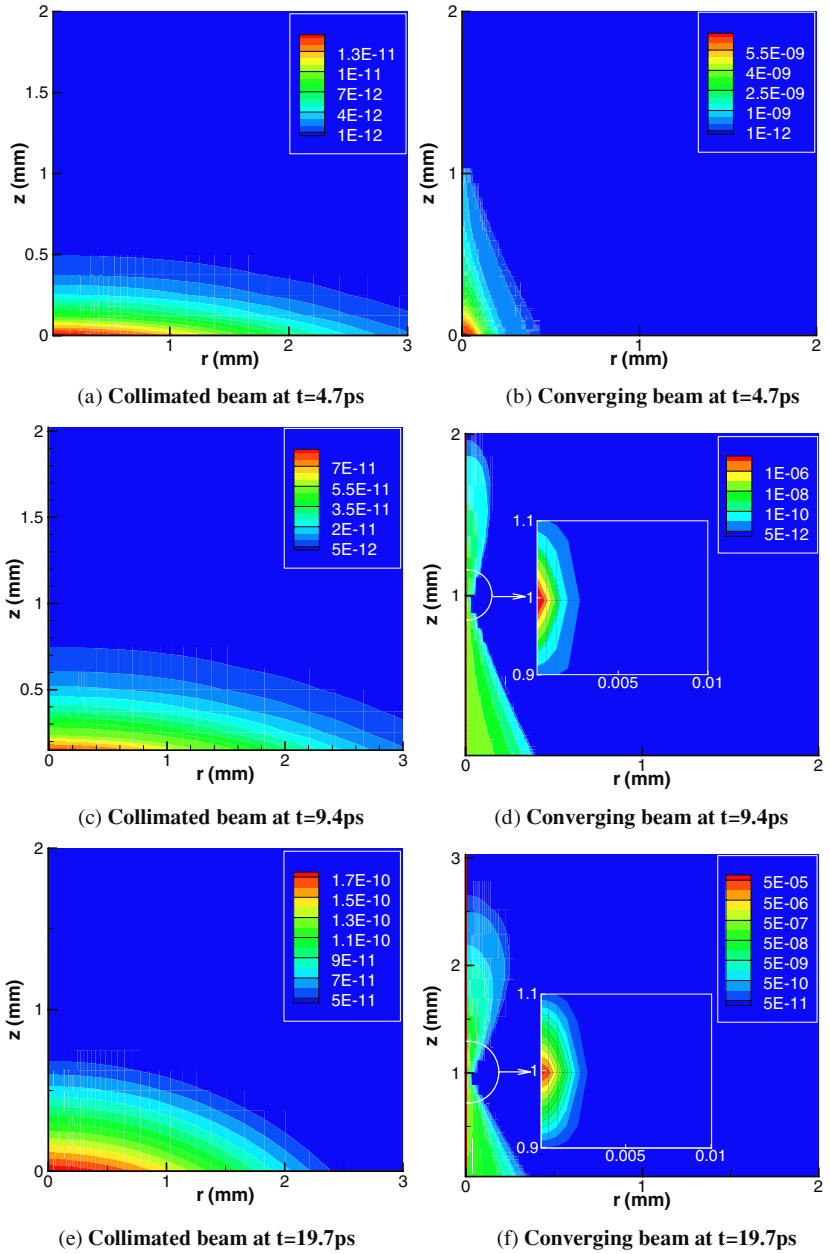

(a) **Collimated beam at t=4.7ps** (b) **Converging beam at t=4.7ps**

(c) **Collimated beam at t=9.4ps** (d) **Converging beam at t=9.4ps**

(e) **Collimated beam at t=19.7ps** (f) **Converging beam at t=19.7ps**

Figure 4. Comparison of radiation propagation between the collimated and focused beams: (a) collimated beam at $t = 4.7$ ps, (b) converging beam at $t = 4.7$ ps, (c) collimated beam at $t = 9.4$ ps, (d) converging beam at $t = 9.4$ ps, (e) collimated beam at $t = 19.7$ ps, (f) converging beam at $t = 19.7$ ps.

that the numerical results calculated with three different grid systems converge to one curve and match well with the exact solutions.

Figure 4 shows the laser intensity contours at three time instants in the skin tissue subjected to one single 10 ps pulse irradiation, in which the collimated and converging beams of the

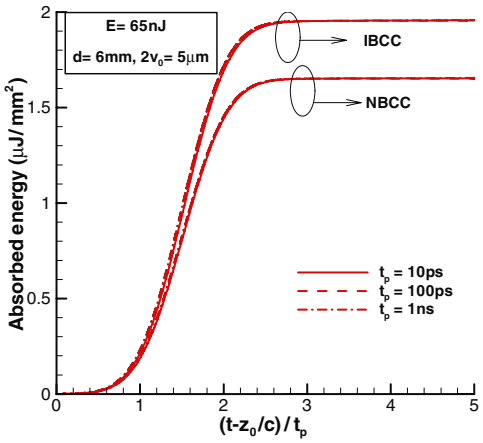

Figure 5. The accumulation of the absorbed radiative energy at the focal spot due to the irradiation of a single pulse.

same power are considered for comparison. An IBCC tumor is located in the region 1–2 mm beneath the skin surface. For the focused beam irradiation, the focal plane is at $z = 1$ mm. Since the speed of light in the skin tissue is approximately 0.21429 mm ps^{-1}, the times for light traveling 1 and 2 mm distances are 4.666 and 9.333 ps, respectively. Figures 4(b), (d) and (f) all show good convergence of the focused laser beam at the focal spot. At $t = 4.7$ ps, the wave front just passed the line $z = 1$ mm. At $t = 9.4$ ps, the wave front passed the line $z = 2$ mm. At $t = 19.7$ ps that is 1.5 t_p plus 4.7 ps, the peak power of the laser arrives at the focal spot. Comparing the focused beam results with the corresponding collimated beam results, it is seen that the focused beam can penetrate a great depth covering the whole tumor region, while the collimated beam can only penetrate a superficial layer to about 0.7 mm beneath the skin surface. The intensity of the focused beam is generally two to five orders of magnitude stronger than that of the collimated beam. In particular, it is seen that the intensity at the focal spot in figure 4(f) is over five orders of magnitude greater than the maximum intensity of the collimated beam. More importantly, the maximum intensity in the collimated beam situation is always at the skin surface, while the focused beam can deliver the maximum power to the target (i.e., the focal spot) inside the tissue. The advantage of the focused beam is then obvious.

Taking the focal spot size as the characteristic length for heat diffusion (L =5.0 μm), the thermal relaxation time in the tumor region is estimated as (Niemz 2002) $\tau = L^2/[4(k/\rho C)_{\text{tumor}}] = 45$ μs. It is much longer than any laser pulse that could be considered as a short pulse. Therefore, the thermal diffusion during a single pulse period is negligible. Then the temperature rise within a pulse irradiation period depends on the totally accumulated energy that is absorbed by the tissue. The profiles of the absorbed radiation energy at the focal spot for the converging laser beam of different pulse widths (10 ps, 100 ps and 1 ns, respectively) are shown in figure 5. The time subtracted by the photon flight time from the surface to the focal spot ($z = 1$ mm) is normalized by the respective laser pulse width. It is found that the absorbed radiative energy accumulates rapidly within one t_p period. After the pulse is off at 3 t_p, the accumulated energy almost saturates. It is reasonable to cut off the transient calculation for one single pulse irradiation after $5t_p$ plus the photon flight time and assume a pseudosteady state is achieved. From figure 5, it is also observed that the radiative energy accumulated in the IBCC-type tumor is larger than that in the NBCC-type tumor because the IBCC has a higher absorption coefficient.

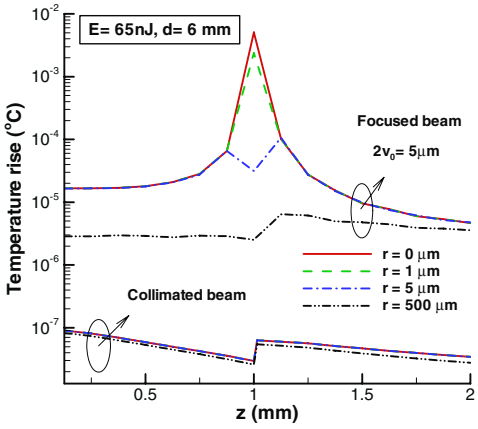

Figure 6. The temperature rise profiles at the end of the irradiation of a single pulse.

Figure 6 shows the temperature rise distributions along the axial direction with four different radial positions for the tissue cylinder subjected to one pulse of either the collimated or converging irradiance. The collimated laser beam is 6 mm in diameter. The focal spot of diameter approximately 5 μm is at the plane $z = 1$ mm. The focused beam radius on the skin surface is then about 210 μm. It is seen that the temperature rise in the tissue along the beam path is several orders of magnitude higher for the focused beam than for the collimated beam. There is an obvious peak rise around the focal spot ($z = 1$ mm, $r < 2.5$ μm). For the collimated irradiance, a small temperature jump is also observed after $z = 1$ mm because of the higher absorption of the IBCC than the epidermis layer in front. However, this temperature jump is still lower than that at the skin surface ($z = 0$). Thus, the skin surface is susceptible to thermal damage during thermal therapy of the tumor if a collimated beam is adopted.

It should be noted that the temperature rise in figure 6 is due to the irradiation of a single pulse. To achieve the target temperature for thermal therapy, continuously repetitive pulses will be needed. It has been discussed earlier that a temperature rise to 56 °C for 1 s or more could be sufficient to kill tumors. In the same time, the temperature cannot rise too high to avoid cell necrosis in the surrounding healthy tissue. A critical temperature of 62 °C corresponding to 25 °C temperature rise is selected as the onset of irreversible tissue damage in this study. Therefore, it is crucial to consider the irradiation of a pulse train with a beam focused to the tumor region to realize a temperature rise in the range between 19 °C and 25 °C for at least 1 s. The temperature used in figures 7 and 9–11 is the volumetrically averaged value over a volume of the focal spot size to facilitate the comparison of others in the future.

Figure 7 shows the transient profiles of temperature rise at four different axial locations in the centerline of the skin tissue cylinder. The beam is focused at $z = 1$ mm. From figure 7(a), it is seen that the temperature rise at the focal spot is the largest. The temperature in the tissue increases as time advances (i.e., with continuous pulse train incidence). For the considered laser power (0.065 W), the temperature rise in the focal spot reaches to19 °C at about 2.6 s and goes over 25 °C at about 4.2 s. Thus, the total time duration in the therapeutic temperature window (56–62 °C) is 1.6 s, longer than the required 1 s. The laser irradiation could be cut off any time between 3.6 and 4.2 s. In the case of $t = 4.2$ s, the skin surface temperature ($z = 0$) is about 55 °C. No irreversible tissue damage occurs. Under the microscopic view in figure 7(b) for the temperature rise in the several initial pulses, it is observed that the temperature actually

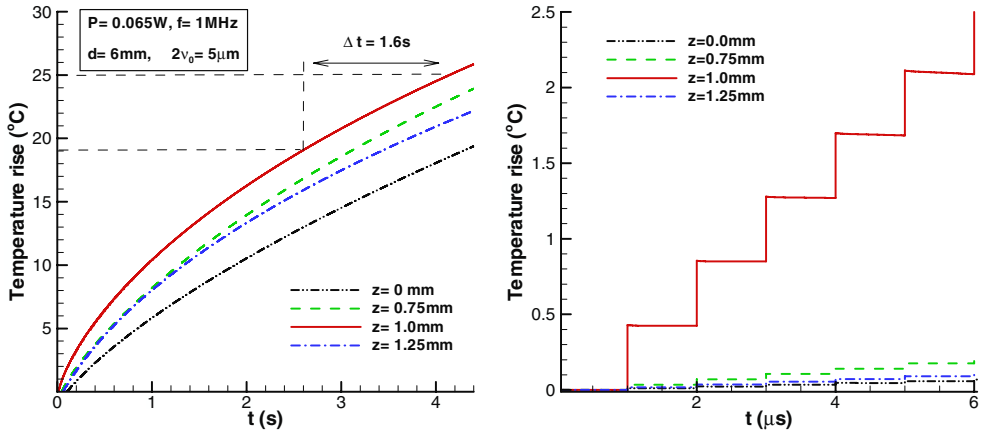

(a) **Meso-time scale** (b) **Micro-time scale**

Figure 7. Transient profiles of the temperature rise due to the irradiation of a pulse train: (a) meso-time scale, (b) micro-time scale.

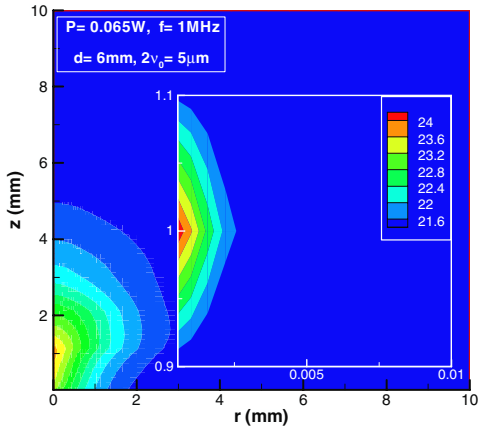

Figure 8. The temperature field at irradiation time instant 4 s.

increases like a staircase. At the onset of each new pulse, there is a clear temperature jump. Further, the temperature rise is substantially larger at the focal spot than other regions at the initial time stage as shown in figure 7(b). This is because the laser energy is focused at the focal spot with negligible heat diffusion. As the time scale collapses, the effect of thermal diffusion is increasingly evident and thus the temperature difference between different locations narrows as shown in figure 7(a).

The contour of temperature rise in the skin tissue with an IBCC-type tumor after 4 s pulse train irradiation (0.065 W) is plotted in figure 8. Inspecting the enlarged view in the focal spot, clearly the temperature is much higher in the focal spot than any other region, including the laser incident surface.

The focal spot size is inversely proportional to the collimated beam diameter before the converging lens. Figure 9 shows the effects of the spot size on (a) the transient temperature profiles at two selected points (incident surface at $z = 0$ and focal plane at $z = 1$ mm) and (b) the temperature profiles along the optical axis at the end of a pulse train ($t = 4$ s). The three

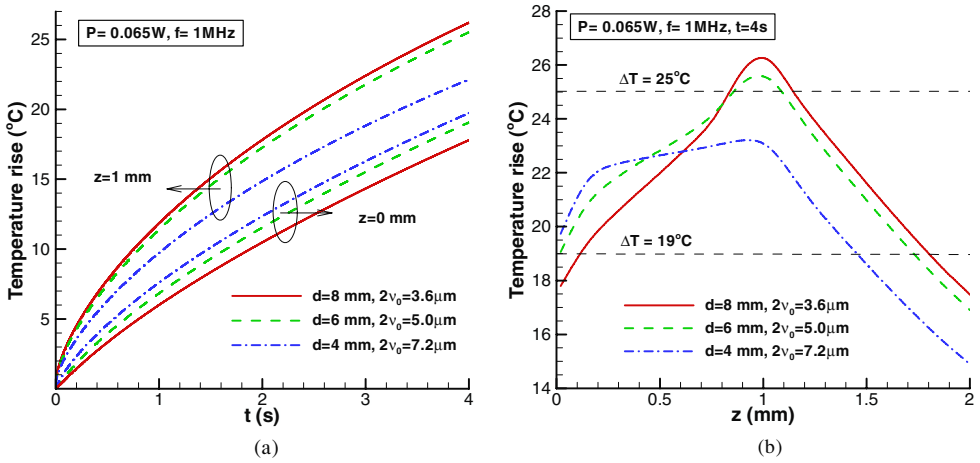

Figure 9. (a) The transient profiles of the temperature rise with different focal spot sizes, and (b) the temperature rise profiles along the optical axis at irradiation time instant 4 s.

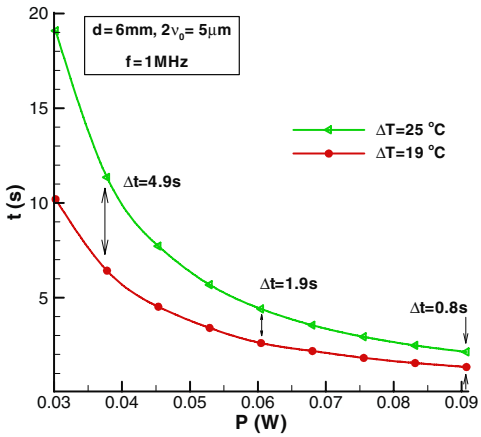

Figure 10. The relationship between the laser power and the irradiation times to achieve the target temperature rise at the focal spot.

selected collimated beams with diameter 4, 6 and 8 mm are converged to spots approximately 7.2, 5.0 and 3.6 μm in diameter, respectively and the impinging areas on the skin surface are calculated as 141, 210 and 275 μm in diameter, respectively. From figure 9(a), it is seen that the focal spot with the smallest diameter is preferred, because the temperature rise at the smallest focal spot is the highest while the temperature rise at the incident skin surface is the lowest in this case. Figure 9(b) also demonstrates this preference because the temperature in most of the epidermis layer before the tumor is the coldest for the smallest focal spot, while the temperature in the tumor region is the highest. Although the temperature rise goes over the 25 °C line for the small spots (3.6 and 5.0 μm), this problem can be resolved via reducing the laser power.

Figure 10 shows the incident laser powers and irradiation times required in order for the temperature at the focal spot to raise 19 °C and 25 °C, respectively. The laser beam

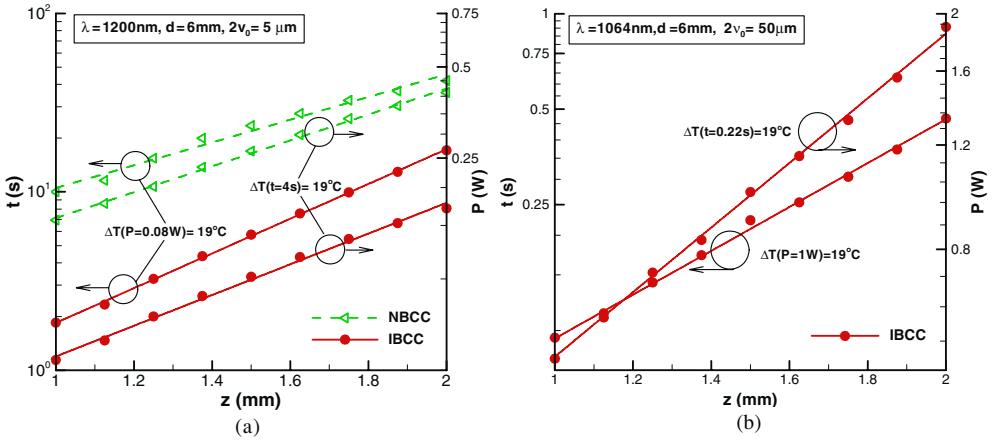

Figure 11. The required laser power or irradiation time for 19 °C temperature rise at the focal spot versus the focal plane location for irradiation: (a) with wavelength at 1200 nm and spot size 5 μm in diameter, and (b) with wavelength at 1064 nm and spot size 50 μm in diameter.

is converged to the tumor edge 1 mm beneath the skin surface, and the focal spot is 5 μm in diameter. The time gap between these two irradiation times is the time duration within the therapeutic temperature window. It is seen that the times required for reaching the two target temperatures decrease as the laser power increases. This decrease is faster for the target temperature rise of 25 °C. Thus, the time period available for safe treatment decreases as the power increases.

In order to completely kill a small skin tumor existing in the dermis layer, the focal spot may have to vary in the axial direction to cover the whole cancerous region. Figure 11 shows the relationships between the focal plane position and the incident laser power required for 19 °C temperature rise at the focal spot at a fixed time instant or the irradiation time required for 19 °C temperature rise at the focal spot with a fixed laser power. Two wavelengths are considered. In figure 11(a), the laser wavelength is 1200 nm and the focal spot size is 5 μm in diameter; in figure 11(b), the laser wavelength is 1064 nm and the focal spot size is 50 μm in diameter. The symbols in the figures represent the data which are calculated by the present model while the lines are obtained by the exponential fitting of the calculated data. To better illustrate the exponential effect, the logarithmic scale is adopted in the Y-coordinate. As shown in figure 11(a), as a result of the attenuation due to absorption and scattering in biological tissues, either the required laser power or irradiation time increases as the focus moves to deep tissue. The required power or irradiation time also depends on the absorption property of the tumor. It is seen that less laser power or irradiation time is required for the IBCC-type tumor because this type of tumor has a larger absorption coefficient than the NBCC-type tumor at the considered laser wavelength. And this fact could also be found by observing the slopes of lines which are characterized by the extinction coefficients ($\sigma_e = \sigma_s + \sigma_a$) of these two types of tumor. Furthermore, there should be a balance of trade-off between the laser power and irradiation time. An increased power reduces the treatment time in the therapeutic temperature window. For example, the power must be less than 0.09 W for the case considered in figure 9; otherwise, the treatment time will be less than 1 s. On the other side, an increased irradiation time reduces the laser efficiency.

Comparing figure 11(b) with figure 11(a), it is found that when the focal spot size increases, the laser power required for the temperature rise increases and the irradiation time decreases.

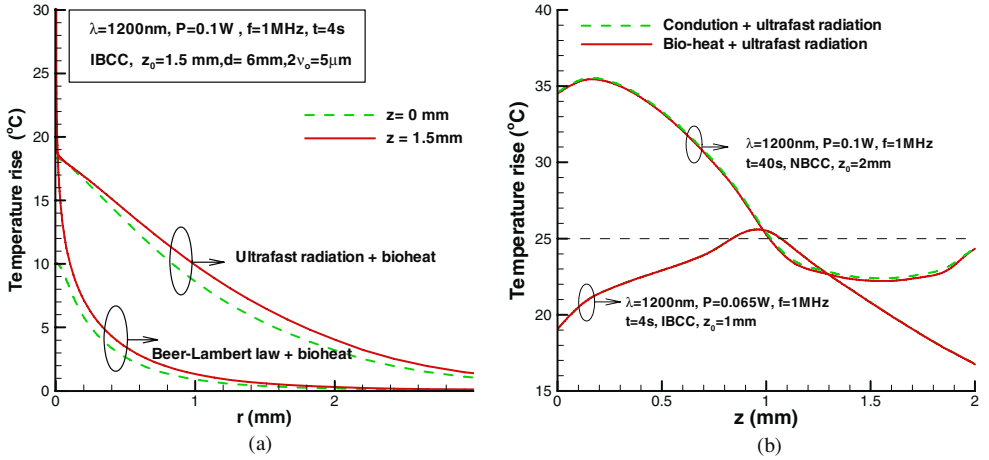

Figure 12. The effects of (a) ultrafast radiation transfer modeling and (b) bio-heat transfer modeling on the predicted temperature profile.

It is of practical interest to estimate how long it would take to destroy a small tumor of 1 mm in radius (R_T) and 1 mm in thickness (H_T). Considering the case with wavelength at 1064 nm and spot size 50 μm in diameter, it takes about 0.223 s to heat up the focal spot by 19 °C and retains for 1 s to completely kill the cancerous cells. The focal depth can be calculated as $2(\Delta z) = \pm 0.64\pi v_0^2/\lambda \approx 1$ mm, covering the whole thickness of the tumor. Thus, the total treatment time is estimated as $(R_T/v_0)^2 \times 1.223 = 1957$ s $= 0.54$ h.

Figure 12(a) shows the radial profiles of the predicted temperatures in the focal plane ($z = z_0 = 1.5$ mm) and the upper surface of the skin tumor ($z = 1$ mm) at time instant 4 s, where the results predicted by the present model (ultrafast radiation + bio-heat) are compared with those calculated by the traditional method (Beer–Lambert law analysis + bio-heat). The simple Beer–Lambert law analysis along the beam path cannot predict accurately the strong scattering of light in biological tissues, resulting in an overestimated temperature rise in the focus and a steeper slope in the temperature radial profile. When an appropriate radiation transfer model is adopted like the present one, the scattering effect will distribute the incident laser power to a larger radial area and result in an extended radial profile. The predicted temperature rise in the focus is over 10 °C low. Hence, the Beer–Lambert law is not a good approximation for light scattering in tissues. Instead the accurate ultrafast radiative heat transfer modeling is necessary.

Finally, the temperature rise along the optical axis predicted by the Pennes bio-heat transfer modeling with blood perfusion and metabolic heat generation is compared in figure 12(b) with that predicted by the pure heat conduction modeling without blood perfusion and metabolic heat generation. The laser wavelength considered is 1200 nm. For the case with focus at the IBCC tumor at $z_0 = 1$ mm, the therapeutic temperature can be realized with a short irradiation time (4 s). It is seen that there is no difference between the two predictions, and thus, the effect of blood perfusion and metabolism is negligible. For the case with focus at the NBCC tumor at $z_0 = 2$ mm, long irradiation time (40 s) is required in order to reach the therapeutic temperature, and there is a minor difference between the two predictions, about 0.2 °C difference in the tumor region. Moreover, the temperature is higher in the front epidermis layer than in the NBCC tumor region because the light absorption for the epidermis is stronger than that for

the NBCC at the wavelength considered. Options to resolve this problem may include: (1) enhancement of the absorption coefficient of the NBCC via administrating absorbing dyes or selecting a different light wavelength and (2) augmentation of the skin surface heat transfer coefficient via cryogen spray cooling or other thermal management techniques.

4. Conclusions

A complete thermal analysis combining the ultrafast radiative heat transfer and transient bio-heat transfer is developed. The model is validated by comparison with exact solutions at steady state for homogeneous cylinders. Thermal modeling of inhomogeneous model skin tissues subjected to pulse train irradiation for thermal therapy is carried out. It is found that pure heat conduction can be a good approximation for short irradiation time, but bio-heat transfer modeling is necessary for accurate prediction of tissue temperature particularly for long irradiation time. The treatment of the focused beam is formulated. As compared with the collimated irradiation, the converging beam can penetrate a greater depth to the desired target region and produce a higher temperature rise at the focal spot than at the skin surface. It leads to localized heating for thermal therapy without concerns of thermal damage to the surroundings.

The laser power or irradiation time required for the temperature in the focal spot rising to the therapeutic temperatures depends on the tumor type, the axial location of the focal plane as well the size of the focal spot. A small focal spot is preferred because it reduces the laser power needed and has a minimal temperature rise in the front epidermis layer. In order to retain at least 1 s irradiation time period in the therapeutic temperature window (56–62 °C) for killing the skin cancers, the current thermal modeling is significant for finding appropriate laser parameters. The model can accurately predict the temperature distribution in the whole tissue cylinder at any time instant.

Acknowledgments

This material is based upon work supported by the National Science Foundation under grant no CBET-0827473.

References

Amin Z, Donald J J, Masters A, Kant R, Lees W and Brown S G 1993 Interstitial laser photocoagulation therapy for liver tumours: clinical results *Proc. SPIE* **1882** 202–9

Anderson D A, Tannehill J C and Pletcher R H 1984 *Computational Fluid Mechanics and Heat Transfer* (Washington, DC: Hemisphere Publishing Corporation)

Anderson R R and Parrish J A 1983 Selective photothermolysis: precise microsurgery by selective absorption of pulsed radiation *Science* **220** 524–27

Anghileri L J and Robert J 1986 *Hyperthermia in Cancer Treatment* (Boca Raton, FL: CRC Press)

Arkin H, Xu L X and Holmes K R 1994 Recent developments in modeling heat transfer in blood perfused tissues *IEEE Trans. Biomed. Eng.* **41** 97–107

Binzoni T, Courvoisier C, Giust R, Tribilon G, Gharbi T, Hebden J C, Leung T S, Roux J and Deply D T 2006 Anisotropic photon migration in human skeletal muscle *Phys. Med. Biol.* **51** N79–90

Chai J C, Lee H S and Patankar S V 1993 Ray effect and false scattering in the discrete ordinates method *Numer. Heat Transfer* B **24** 373–89

Cohen M L 1977 Measurement of the thermal properties of human skin *J. Invest. Dermatol.* **69** 333–8

Emery A F and Sekins K M 1982 The use of heat transfer principles in designing optimal diathermy and cancer treatment modalities *Int. J. Heat Mass Transfer* **25** 823–34

Gao F, Zhao H J, Tanikawa Y and Yamada Y 2004 Optical tomographic mapping of cerebral haemodynamics by means of time-domain detection: methodology and phantom validation *Phys. Med. Biol.* **49** 1055–78

Gilchrest B A, Eller M S, Geller A C and Yarr M 1999 The pathogenesis of melanoma induced by ultraviolet radiation *N. Engl. J. Med.* **340** 1341–8

Guo Z and Kumar S 2000 Equivalent isotropic scattering formulation for transient radiative transfer in anisotropic scattering planar media *Appl. Opt.* **39** 4411–7

Guo Z, Kumar S and San K-C 2000 Multi-dimensional Monte Carlo simulation of short pulse laser radiation transport in scattering media *J. Thermophys. Heat Transfer* **14** 504–11

Guo Z and Kumar S 2001a Radiation element method for transient hyperbolic radiative transfer in plane-parallel inhomogeneous media *Numer. Heat Transfer* B **39** 371–87

Guo Z and Kumar S 2001b Discrete-ordinates solution of short-pulsed laser transport in two-dimensional turbid media *Appl. Opt.* **40** 3156–63

Guo Z and Kumar S 2002 Three-dimensional discrete ordinates method in transient radiative transfer *J. Thermophys. Heat Transfer* **16** 289–96

Guo Z, Wan S K, August D A, Ying J, Dunn S M and Semmlow J L 2006 Optical imaging of breast tumor through temporal log-slope difference mappings *Comput. Biol. Med.* **36** 209–23

Hebden J C, Arridge S R and Delpy D T 1997 Optical imaging in medicine: I. Experimental techniques *Phys. Med. Biol.* **42** 825–40

Jeong S W, Liu H and Chen W R 2003 Temperature control in deep tumor treatment *Proc. SPIE* **5068** 210–6

Kim K H and Guo Z 2004 Ultrafast radiation heat transfer in laser tissue welding and soldering *Numer. Heat Transfer* A **46** 23–40

Kim K and Guo Z 2007 Multi-time-scale heat transfer modeling of turbid tissues exposed to short-pulsed irradiations *Comput. Methods Programs Biomed.* **86** 112–23

Manns F, Milne P J, Gonzalez-Cirre X, Denham D B, Parel J M and Robinson D S 1999 *In situ* temperature measurements with thermocouple probes during laser interstitial thermometry (LITT): quantification and correction of a measurement artifact *Lasers Surg. Med.* **23** 94–103

Mitra K and Kumar S 1999 Development and comparison of models for light pulse transport through scattering absorbing media *Appl. Opt* **38** 188–96

Niemz M H 2002 *Laser-Tissue Interactions: Fundamentals and Applications* (Berlin: Springer)

Ntziachristos V, Yodh A G, Schnall M and Chance B 2000 Concurrent MRI and diffuse optical tomography of breast after indocyanine green enhancement *Proc. Natl Acad. Sci. USA* **97** 2767–72

Pfefer T J, Smithies D J, Milner T E, van Gemert M J C, Nelson J S and Welch A J 2000 Bioheat transfer analysis of cryogen spray cooling during laser treatment of port wine stains *Lasers Surg. Med.* **26** 145–57

Quan H and Guo Z 2004 Fast 3-D optical imaging with transient fluorescence signals *Opt. Exp.* **12** 449–57

Robinson D S, Parel J M, Denham D B, Gonzalez-Cirre X, Manns F, Milne P J, Schachner R D, Herron A J, Comander J and Hauptmann G 1998 Interstitial laser hyperthermia model development for minimally invasive therapy of breast carcinoma *J. Am. Coll. Surg.* **186** 284–92

Salomatina E, Jiang B, Novak J and Yaroslavsky A N 2006 Optical properties of normal and cancerous human skin in the visible and near infrared spectral range *J. Biomed. Opt.* **11** 261–9

Sassaroli A, Martelli F, Imai D and Yamada Y 1999 Study on the propagation of ultra-short pulse light in cylindrical optical phantoms *Phys. Med. Biol.* **44** 2747–63

Wan S K, Guo Z, Kumar S, Aber J and Garetz B A 2004 Noninvasive detection of inhomogeneities in turbid media with time-resolved log-slope analysis *J. Quant. Spectrosc. Radiat. Transfer* **84** 493–500

Wu S C and Wu C H 1997 Radiative heat transfer in a two-dimensional cylindrical medium exposed to collimated radiation *Int. Commun. Heat Mass Transfer* **24** 475–84

Yamada Y 1995 Light-tissue interaction and optical imaging in biomedicine *Annu. Rev. Heat Transfer* **6** 1–59

Yamada Y 2000 Fundamental studies of photon migration in biological tissues and their application to optical tomography *Opt. Rev.* **7** 366–74

Zhu L, Xu L X, He Q and Weinbaum S A 2002 New fundamental bioheat equation for muscle tissue: part II. Temperature of SAV vessels *ASME J. Biomech. Eng.* **124** 121–32

Zysset B, Fujimoto J G and Deutsch T F 1989 Time-resolved measurements of picosecond optical breakdown *Appl. Phys* B **48** 139–47